NANOMEDICINE

Inhalation of peptide-loaded nanoparticles improves heart failure

Michele Miragoli,[1,2,3]*† Paola Ceriotti,[1,3]* Michele Iafisco,[4] Marco Vacchiano,[1] Nicolò Salvarani,[1,3] Alessio Alogna,[5,6] Pierluigi Carullo,[1,3] Gloria Belén Ramirez-Rodríguez,[4] Tatiana Patrício,[4] Lorenzo Degli Esposti,[4] Francesca Rossi,[7] Francesca Ravanetti,[8] Silvana Pinelli,[2] Rossella Alinovi,[2] Marco Erreni,[1,9] Stefano Rossi,[2] Gianluigi Condorelli,[1,3,9] Heiner Post,[5,10] Anna Tampieri,[4] Daniele Catalucci[1,3]†

Peptides are highly selective and efficacious for the treatment of cardiovascular and other diseases. However, it is currently not possible to administer peptides for cardiac-targeting therapy via a noninvasive procedure, thus representing scientific and technological challenges. We demonstrate that inhalation of small (<50 nm in diameter) biocompatible and biodegradable calcium phosphate nanoparticles (CaPs) allows for rapid translocation of CaPs from the pulmonary tree to the bloodstream and to the myocardium, where their cargo is quickly released. Treatment of a rodent model of diabetic cardiomyopathy by inhalation of CaPs loaded with a therapeutic mimetic peptide that we previously demonstrated to improve myocardial contraction resulted in restoration of cardiac function. Translation to a porcine large animal model provides evidence that inhalation of a peptide-loaded CaP formulation is an effective method of targeted administration to the heart. Together, these results demonstrate that inhalation of biocompatible tailored peptide nanocarriers represents a pioneering approach for the pharmacological treatment of heart failure.

INTRODUCTION

The application of nanotechnology to medicine (nanomedicine) is at the forefront of innovation for modern health care and represents a promising approach for efficient delivery of therapeutics (*1*–*3*). In line with this, a collection of first-generation nanoproducts for clinical use have recently been approved by the U.S. Food and Drug Administration, and other liposomal and polymer drug conjugate nanosystems are under clinical and preclinical development (*4*–*7*). However, despite remarkable advances in the use of nanoparticles in the cancer field, very few preclinical tests have been reported for nanomedicine applied to the treatment of cardiovascular diseases (CVDs) (*8*–*10*) that, claiming 17.5 million lives a year and accounting for an estimated 31% of all deaths globally, stand as the leading cause of death worldwide (*11*). The identification of innovative therapeutic nanoformulations, use of alternative administration routes, or a combination of both may help to overcome the limitations associated with current pharmacological treatments for CVDs and lead to more specific and efficient therapies.

Drug administration for the treatment of myocardial disease currently includes either oral or needle-based routes (*12*). However, enteral resorption is unreliable during acute or chronic gastrointestinal congestion, whereas injection, either intravenous, subcutaneous, or intramuscular, is associated with patient discomfort and malcompliance, rendering these administrations suboptimal for chronic treatment. Moreover, home or ambulatory care is frequently required for injection procedures. To the best of our knowledge, no study has addressed the possibility of using nanoparticles that can treat cardiac conditions when inhaled. Although inhalation delivery is a common procedure for the treatment of respiratory problems, no pharmacological therapies are, as far as we know, currently adopting an inhalation approach for the delivery of therapeutics via nanoparticles to the heart. Furthermore, despite an increasing interest in peptide therapeutics in pharmaceutical research and development, no effective, noninvasive, peptide-based treatment of cardiac dysfunction has been successfully developed so far, leaving the parental route (injection) the only currently available option (*13*, *14*).

Here, we show that inhalation therapy is effective for delivering nanoparticle-based therapeutic peptide to the diseased heart. The approach is based on our previously described biocompatible and biodegradable, negatively charged calcium phosphate nanoparticles (CaPs) that, via a biomineralization-inspired strategy, are produced with a diameter ranging from 20 to 50 nm and are able to deliver bioactive molecules to cardiac cells (*15*). Without promoting toxicity or interfering with any functional properties of cardiomyocytes, CaPs were shown in vitro to successfully cross the cardiomyocyte cellular membrane and release bioactive molecules (microRNAs) inside the cell (*15*). We thus sought to assess whether the cardiac targeting of CaPs could be applied for the delivery of therapeutic peptides via the respiratory tree through inhalation (Fig. 1A). The rationale for the use of this unconventional administration route for targeting of the heart is based on the concepts that (i) during respiration the oxygenated blood moves from the pulmonary circulation first to the heart via the pulmonary vein and (ii) combustion-derived nanoparticles and ultrafine particulates inhaled through polluted air were recently shown by us (*16*) and others (*17*) to be present in the heart and causally associated with cardiac arrhythmia and dysfunction,

[1]Humanitas Clinical and Research Center, Rozzano, Milan 20089, Italy. [2]Department of Medicine and Surgery, University of Parma, Parma 43126, Italy. [3]Institute of Genetics and Biomedical Research, Milan Unit, National Research Council, Milan 20138, Italy. [4]Institute of Science and Technology for Ceramics, National Research Council, Faenza, Ravenna 48018, Italy. [5]Department of Internal Medicine and Cardiology, Campus Virchow Klinikum, Charité University Medicine Berlin, Berlin 13353, Germany. [6]Berlin Institute of Health, Berlin 10117, Germany. [7]Institute of Materials for Electronics and Magnetism, National Research Council, Parma 43126, Italy. [8]Department of Veterinary Science, University of Parma, Parma 43126, Italy. [9]Humanitas University, Rozzano, Milan 20089, Italy. [10]Department of Cardiology, Contilia Heart and Vessel Centre, St. Marien-Hospital Mülheim, Mülheim 45468, Germany.
*These authors contributed equally to this work.
†Corresponding author. Email: michele.miragoli@humanitasresearch.it (M.M.); daniele.catalucci@cnr.it (D.C.)

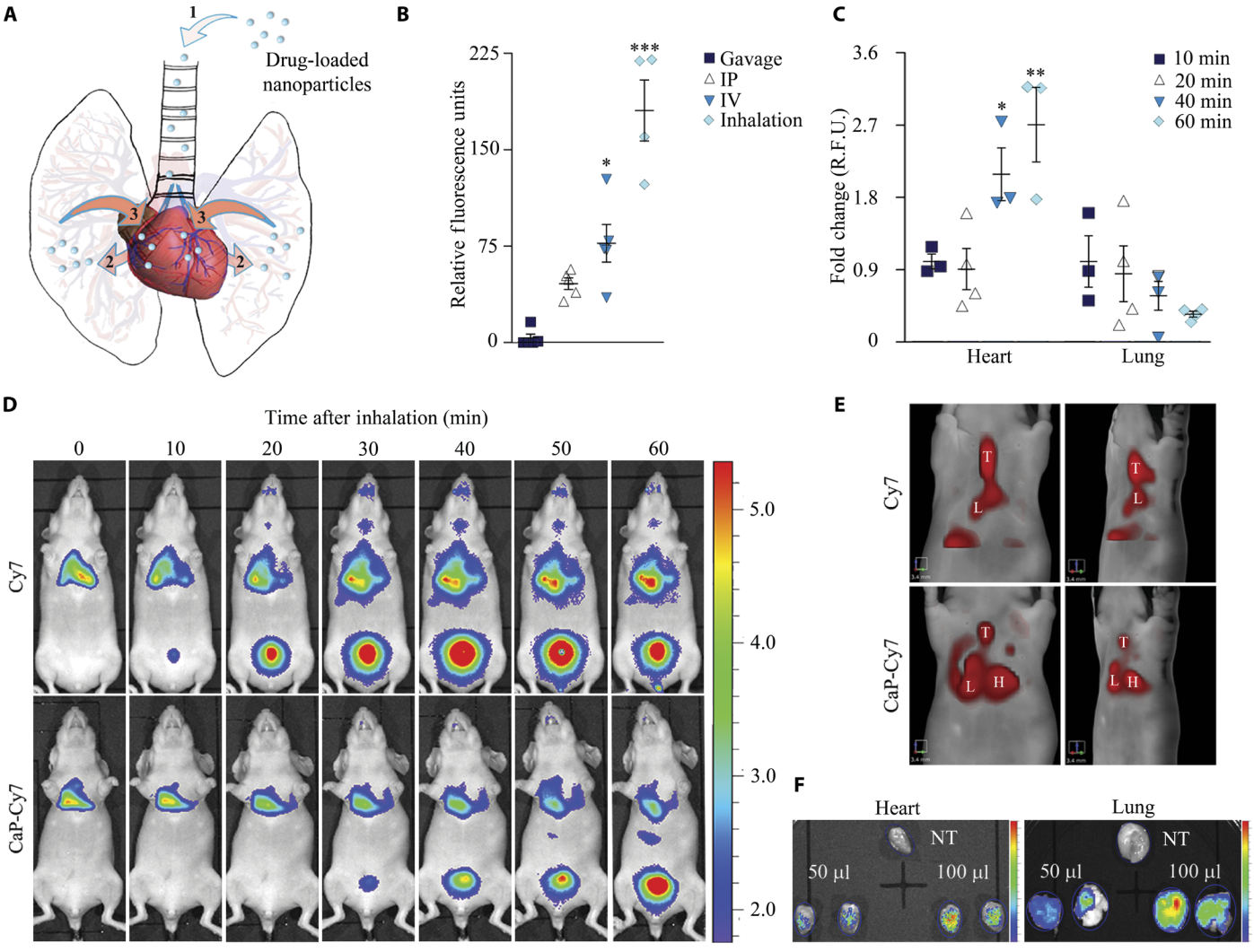

Fig. 1. Inhalation delivers CaPs to the heart. (**A**) Schematic representation of CaP heart targeting via the inhalation route. 1, nanoparticle inhalation; 2, nanoparticle deposition in lungs and translocation through the air-blood pulmonary barrier; 3, heart targeting and drug release into the heart. (**B**) Quantification of Cy7 fluorescence signals from heart tissue of mice treated with CaP-Cy7 via gavage, intraperitoneal (ip), intravenous (iv), and inhalation administration. Data are means ± SEM. $^{*}P < 0.05$ and $^{***}P < 0.001$ compared to gavage [one-way analysis of variance (ANOVA) test] ($n = 5$). (**C**) Time-course quantification of Cy7 fluorescence signals from heart and lung tissue of mice treated with CaP-Cy7 via inhalation administration. Data are means ± SEM. $^{*}P < 0.05$ and $^{**}P < 0.01$ compared to the 10-min time point (two-way ANOVA test) ($n = 5$). R.F.U., relative fluorescence units. (**D**) Whole-body optical in vivo imaging to evaluate the distribution of CaP-Cy7 and Cy7 in CD1 nude mice at different time points after inhalation. Data are representative of at least six independent experiments. Values are expressed as radiance efficiency ($\times 10^9$). (**E**) 3D FMT imaging of mice as presented in (D) and analyzed 60 min after CaP-Cy7 and Cy7 administration. T, trachea; H, heart; L, lung. (**F**) Fluorescence imaging of explanted hearts from perfused mice analyzed 60 min after inhalation of 50 and 100 µl of CaP-Cy7. NT, heart from nontreated mouse. Values are expressed as radiance efficiency. Scale values: heart, 1.04×10^7 (maximum) to 3.56×10^6 (minimum); lung, 7.78×10^7 (maximum) to $6.17 \times 10^{6.9}$ (minimum) ($n = 4$).

suggesting that inhaled nanoparticles are deposited in the heart. Furthermore, CaPs can protect peptides from immediate enzymatic degradation and, because of their negative surface charge, provide cellular permeability via the membrane internalization (*15*, *18*). Thus, we predicted that inhaled small-sized CaPs would be able to cross the alveolar-capillary barrier in the lung and rapidly translocate to the myocardium for effective intracellular release of therapeutic peptides.

RESULTS

Characterization of inhalable CaPs

Before in vivo administration, CaPs were subjected to a set of in vitro evaluation procedures. First, long-term stability in aqueous suspension was assessed by measurement of CaP surface charge and Z-average as a function of time as well as CaP interaction with proteins. No changes were found in the surface charge, which remained stable (−32 ± 3 mV) for the whole time of investigation, whereas the initial Z-average value of about 125 nm was found to decrease to about 80 nm after 2 days of storage at 4°C (fig. S1A). Thereafter, Z-average value remained stable with only minor variations (±10 nm) for up to 8 days, which was the time limit for our investigation. To evaluate the potential interaction of proteins with CaPs, nanoparticles were analyzed in aqueous suspension enriched with 10% (v/v) fetal bovine serum (FBS) (fig. S1B). Z-average decreased from about 80 nm (in pure water) to about 32 nm, indicating that serum proteins interacting with the nanoparticles increased the dispersion of CaPs. Thereafter,

a gradual increase in Z-average was registered, reaching a value of about 280 nm after 7 days. At this later time point, an increment of the ζ-potential from −30 to −10 mV corroborated the expected surface interaction of CaPs with proteins. Together, these data show that no substantial size alterations occur within the first hours, suggesting that an in vivo administration featuring a fast targeting of the heart might not face any alteration of CaP properties.

In a second step, near-infrared fluorophore-loaded CaPs [CaP–cyanine 7 (Cy7)] were generated for in vivo biodistribution analyses, and the effective encapsulation of the fluorophore in the CaPs as well as the stability of CaP-Cy7 were demonstrated (fig. S1C). To determine the effective incorporation of Cy7 into CaPs, comparable amounts of Cy7 were either encapsulated into (CaP-Cy7) or adsorbed after synthesis to CaPs, and the amount of CaP-associated Cy7 was measured, revealing an amount of 1.40 ± 0.13% (w/w) encapsulated CaP-Cy7 versus 0.85 ± 0.08% (w/w) CaP adsorbed after synthesis. The analysis of the surface charge of CaP-Cy7 at pH 7.4 revealed the presence of a single population with surface charge of about −20 mV, whereas CaPs with the fluorophore adsorbed on their surface showed a double population with surface charge of about −34 and −6 mV attributed to naked CaPs and fluorophore-coated CaPs (fig. S1C). These data support the conclusion that, when included during the synthesis of nanoparticles, Cy7 is effectively encapsulated within the CaPs and not attached to the surface. In addition, CaP-Cy7 did not show any release of fluorophore (limit of detection of 1 μg/ml) against an infinite sink in dialysis as well as in aqueous suspension enriched with 10% (v/v) FBS.

Delivery of CaPs to the heart by inhalation

After CaP generation and characterization, we assessed the possibility of heart targeting by nanoparticle administration. CaP-Cy7 were delivered to healthy mice, and fluorescence measurements were performed to compare distinct administration routes, which, in addition to conventional ways [oral (gavage), intraperitoneal, and intravenous], included nebulization of CaP-Cy7 via the respiratory route. Whereas enteral administration (gavage) did not result in statistically significant ($P > 0.05$) targeting to the heart at 40 min after administration, parenteral administration (intraperitoneal and intravenous) and inhalation resulted in rapid delivery of CaP-Cy7 to the myocardium, with inhalation being the most efficient delivery method (Fig. 1, B and C, and fig. S2, A to D). Notably, the time course of CaP-Cy7 myocardial accumulation was paralleled by a gradual reduction in signal from the lungs as a function of time, suggesting a continuous passage of nanoparticles across the pulmonary barrier (Fig. 1C). Similar results were obtained via an optical in vivo imaging approach, which allowed us to monitor the behavior of inhaled CaP-Cy7 and their gradual accumulation in the mediastinum, the thoracic cavity containing the heart, esophagus, and trachea (Fig. 1D and fig. S2B). A delayed clearance of inhaled CaP-Cy7 was observed compared to Cy7 alone (Fig. 1D and fig. S2E), which was supported by three-dimensional (3D) fluorescence molecular tomography (FMT) imaging of the cardiopulmonary area from mice 60 min after inhalation, revealing marked localization of CaP-Cy7 in the myocardium compared to Cy7 alone (Fig. 1E and movies S1 and S2). Effective delivery of CaP-Cy7 to the myocardium was further confirmed by fluorescence analyses on explanted hearts (Fig. 1F), whereas no specific cardiac targeting was found in Cy7 alone, which rapidly accumulated in the bladder after rapid and broad diffusion in the lungs and in the rest of the body (Fig. 1, D to F). In addition, no CaP-Cy7s were found to cross the blood-brain barrier (Fig. 1D and fig. S2C). Targeting of CaPs to the myocardium was also confirmed by transmission electron microscopy (TEM) (fig. S2, F and G). Notably, in contrast to the toxic outcome associated with inhalation of ultrafine particulates from polluted air and other inorganic nanoparticles such as TiO_2, SiO_2, and Co_3O_4 nanoparticles (*19*–*22*), pulmonary CaP administration via single or multiple once-a-day administration protocols did not affect cardiac function as measured by echocardiography (fig. S3 and table S1). In rats, no alterations in cardiac excitability and refractoriness were detected as shown by the absence of arrhythmogenic events evaluated by in vivo epicardial multiple lead recordings (table S2). Furthermore, no immunological effects were observed, as indicated by no detectable changes in RNA expression of CD11, interleukin-1 (IL-1), tumor necrosis factor (TNF), IL-6, IL-4, and IL-5. In agreement with our recent work (*15*), this evidence supports the concept that biomimetic CaPs, closely resembling the inorganic phase of bone and teeth (*23*), are recognized by the body as close to endogenous material, thus being biocompatible and well tolerated in vivo.

Efficacy of CaPs to load therapeutic peptides

On the basis of our demonstration that CaP inhalation allows nanoparticles to cross the pulmonary barrier and reach the intracellular compartment within the heart, our next objective was to explore the use of peptide-loaded CaPs for cardiac treatment in vivo. We recently demonstrated the therapeutic effect of a cell-penetrating mimetic peptide (R7W-MP) that, by targeting the $Ca_V\beta 2$ cytosolic subunit of the L-type calcium channel (LTCC), improves cardiac contractility in pathological heart conditions associated with alterations of LTCC levels and function (diabetic cardiomyopathy) via restoration of LTCC density at the plasma membrane (*24*). Here, we envisioned to test the therapeutic use of CaPs for peptide delivery for the treatment of a cardiac condition via inhalation of CaPs loaded with R7W-free MP (CaP-MP). Because of the absence of the cell-internalizing R7W sequence on the MP, its efficiency in rescuing cardiac contractility would require the CaPs to mediate its crossing of the pulmonary barrier and subsequent myocardial cell internalization.

In our previous study (*15*), CaPs were functionalized with different quantities of microRNA, revealing a slight increase in CaP size as a function of microRNA amount, whereas comparable values to those of microRNA-free CaPs were obtained for the surface charge and morphology. Here, we performed a similar evaluation and characterized the effect of MP and hemagglutinin (HA) scramble peptides, on size and surface of loaded CaPs. Notably, because our approach is based on a universal nature-inspired synthetic strategy, we found that the incorporation mechanism for peptides into CaPs was similar to the one previously observed for microRNAs. This mechanism consists of a first step of interaction in which, within a basic reaction environment (pH 8.5), the Ca^{2+} and/or PO_4^{3-} ions interact via a strong electrostatic interaction with the chemical groups (carboxylate, amine, and sulfonic groups) of the analyzed biomolecules. Whereas, in the case of Cy7, mainly sulfonic and amine groups are likely to be involved in the interaction, the negative charge of MP and HA peptides, which at the pH of the reaction have a calculated isoelectric point of 7.06 (*25*), generally interacts with Ca^{2+} ions. Afterward, the reaction of PO_4^{3-} with Ca^{2+} ions or vice versa triggers the nucleation of particles and their growth, resulting in the mineralization of biomolecules (creation of a matrix of mineral phase surrounding the biomolecule-rich nucleus). During this process, citrate stabilizes

the nanoparticles and modulates their growth through its binding on the surface at the early stage of crystallization, as previously reported (*15*).

In line with our previous results obtained with microRNA (*15*), immediately after dialysis, higher Z-average, but similar surface charge, was obtained for functionalized CaPs compared to peptide-free CaPs. CaP-MP and CaP-HA showed comparable values of surface charges (−31 ± 2 mV and −32 ± 1 mV), respectively, indicating that their surface is homogenously covered with citrate. Z-averages for the functionalized CaP-MP and CaP-HA were 210 ± 6 nm and 220 ± 6 nm, respectively, where the effective interaction of peptides with CaPs might be responsible for the slight difference in size with respect to peptide-free CaPs (125 nm). Also in this case, the Z-average of CaP-HA and CaP-MP immediately after dialysis decreased as a function of time, passing from about 200 to 90 nm after 2 days (fig. S1A). This value remained stable with small variation (±10 nm) for up to 8 days, which was the time limit for our investigation. Consistently, also in this case, the surface charge of the CaP peptides (−31 ± 3 mV) did not change as a function of time. TEM images of CaP-MPs and CaP-HAs (fig. S4A) collected immediately after dialysis showed round-shaped particles of about 20 to 50 nm in diameter. The selected area electron diffraction patterns collected from the same CaPs (fig. S4A) demonstrated their amorphous nature due to the presence of diffuse rings rather than spots. In addition, energy-dispersive x-ray spectrometry spectra (fig. S4A) revealed that both CaP-MP and CaP-HA are mainly composed of calcium and phosphate. All these features are comparable with our previously prepared CaPs (*15*), and we therefore assumed that the functionalized CaPs synthesized in this work have similar behavior toward cardiomyocytes and cardiac tissue.

To evaluate peptide loading, the total MP in CaP-MP preparations was quantified. To distinguish the amount of CaP-loaded MP from the possible CaP-free MP present in the preparations, peptide quantification was performed from both pellet (CaP-MP) and supernatant (CaP-free MP) fractions obtained by centrifugation. Finally, acidic treatment was performed to completely dissolve CaP-MPs from both fractions, thereby facilitating the total release and effective quantification of total MP. The same approach was used for both the pre- and post-dialysis preparations, and data were compared to the theoretical maximum loading. As shown in table S3, MP loading from the pellet fraction (corresponding to the CaP-loaded MP) was comparable to the theoretical value, leading to the conclusion that CaP provides high loading capacity, keeping the amount of unloaded peptide (CaP-free MP) at a minimum.

To evaluate MP stability within nanoparticles, peptide quantification was performed on CaP-MP aliquots stored at different amounts of time at room temperature using the approach described previously. As shown in fig. S4B, no reduction in MP loading was found until 10 hours of storage at room temperature, whereas a slight decrease was observed at 24 hours of storage, supporting the conclusion that CaP-MPs stably maintain their payload in an encapsulated state. Thereafter, after a time-dependent response to CaP dissolution under acidic conditions, we evaluated release kinetics of encapsulated peptide from nanoparticles. As shown in fig. S4C, a gradual release of MP from CaP-MPs was obtained, showing an inverse relationship between the reduction in the pellet fraction (CaP-loaded MP) and an increase in the supernatant fraction (CaP-free MP). These data are in line with results from inductively coupled plasma optical emission spectrometry (ICP-OES) analyses (fig. S4D) that, by measuring the cumulating Ca^{2+} ion release under physiological (pH 7.4) and slightly acidic (pH 5.5) conditions, provide degradation rate of CaPs and peptide-loaded CaPs as a function of time. Degradation and consequently peptide release are triggered by a drop in pH. Together, these data provide the evidence that CaPs have high loading capacity, keeping the amount of unloaded peptide (CaP-free MP) at a minimum.

Efficacy of inhaled CaPs loaded with a therapeutic MP to improve myocardial contraction

To test the therapeutic use of CaP-MPs for the treatment of a cardiac condition, we treated a mouse model of streptozotocin (STZ)–induced diabetic cardiomyopathy via inhalation of CaPs loaded with R7W-free therapeutic peptide. Consistent with the ability of CaPs to mediate cardiomyocyte internalization (*15*), stimulated emission depletion (STED) 3D z-stack microscopy of isolated adult cardiomyocytes from mice subjected to inhalation of MP-rhodamine–loaded CaPs showed effective targeting of MP to cardiomyocytes, accounting for 124 ± 52 fluorescent signals (corresponding to the internalized MP-rhodamine–loaded CaPs) per single cell (Fig. 2, movie S3, and fig. S5). In agreement with this, CaP-MP inhalation treatment of diabetic mice (Fig. 3A and fig. S6, A and B) led to a complete recovery of cardiac function as shown by echocardiographic assessment of left ventricular (LV) function (Fig. 3B and table S4). Improvement of molecular and cellular defects associated with diabetic cardiomyopathy was achieved as a result of the direct targeting of MP to LTCC (*24*), including restoration of LTCC protein levels (Fig. 3C and fig. S6C), recovery of LTCC currents (Fig. 3D, fig. S6D, and table S5), and LTCC-related contractile properties (Fig. 3E) as determined in isolated cardiomyocytes from CaP-MP–treated mice. In contrast, as expected, no therapeutic effects were obtained by administration of CaP-HA or unloaded (free) MP (Fig. 3, B to E; fig. S6D; and table S4). In addition, no induction of oxidative stress was observed (table S6). Together, these data provide evidence that inhalation of MP-loaded CaPs is an effective approach for delivery of therapeutic peptides to the heart (Fig. 3F) and demonstrate the benefit of CaP-MP inhalation in recovering LTCC-associated cardiac dysfunctions.

Effectiveness of peptide-loaded CaP formulation for targeted administration to the heart in a porcine model

Finally, to advance toward clinical research in humans and generate the first proof of concept in large animals, feasibility of cardiac targeting via our nanoparticle-based inhalation approach was assessed by nebulization of CaP-HA in anesthetized healthy landrace pigs (Fig. 4A). Similar to our results in mice, no changes in heart rate, mean arterial blood pressure, cardiac output (9.8 ± 0.8 versus 9.9 ± 0.8 liters min^{-1}), or systemic and pulmonary vascular resistance were observed 5 hours after a single inhalation of CaP-HA (Fig. 4B). LV function, as assessed by hemodynamic measurements of pressure-time–derived parameters (LV maximum pressure, maximum and minimum LV dP/dt) and pressure-volume analyses (end-diastolic and end-systolic pressure-volume relationships), did not change (Fig. 4C). No arrhythmia occurred, and surface electrocardiography (ECG)–derived PQ (133 ± 6 versus 135 ± 5 ms), QT intervals (349 ± 12 versus 345 ± 19 ms), and QRS duration (56 ± 5 versus 51 ± 5 ms) remained constant. Finally, respiratory function (end-tidal carbon dioxide partial pressure and arterial oxygen saturation) remained stable at constant mechanical respiration. In a separate group of

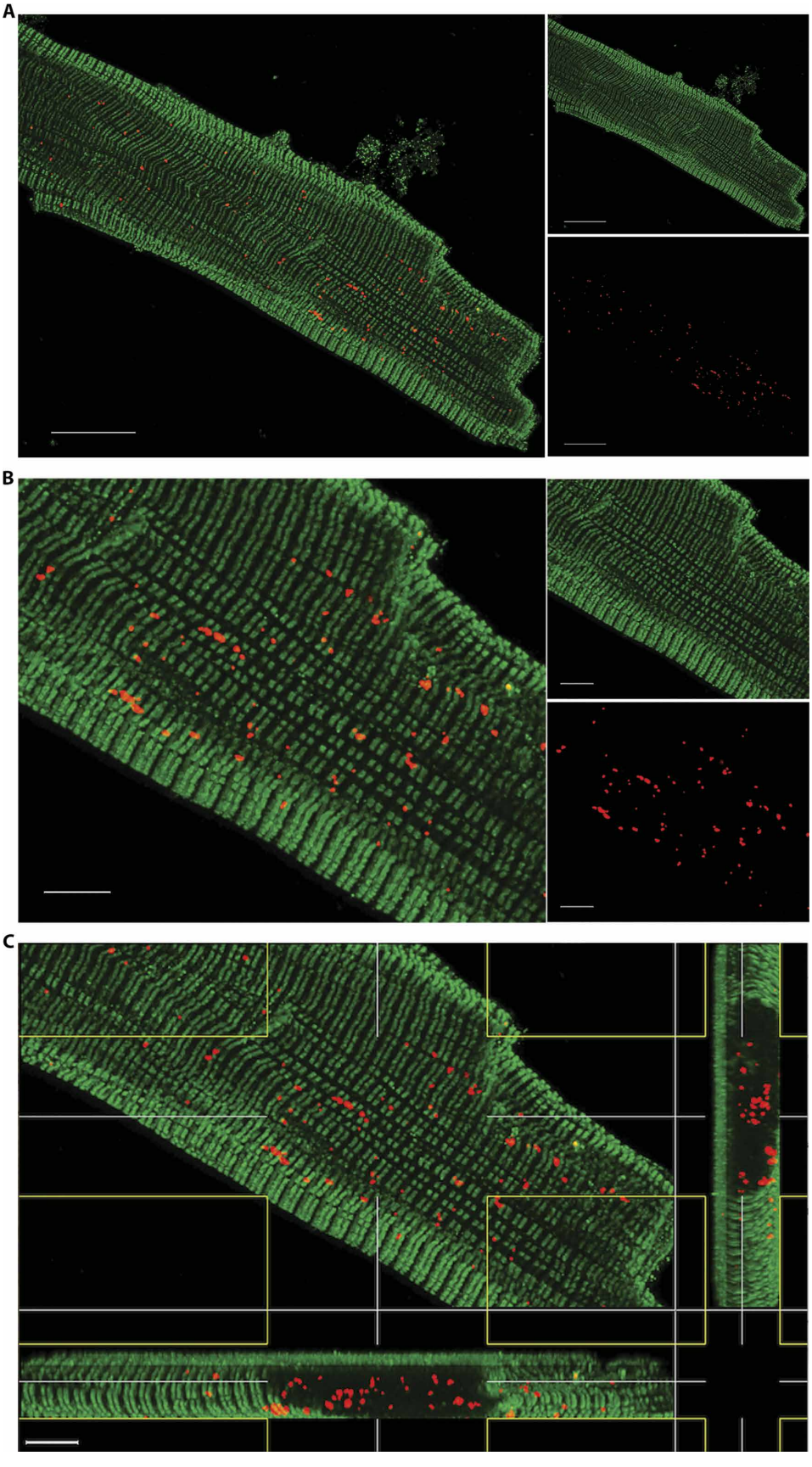

Fig. 2. STED microscopy of isolated cardiomyocytes from mice treated with MP-rhodamine–loaded CaPs. (**A**) STED microscopy on an isolated cardiomyocyte from mice treated with MP-rhodamine–loaded CaPs. Green, LTCC; red, MP-rhodamine. Representative of 10 different acquisitions. Original magnification, ×100; scale bars, 15 μm. (**B**) Enlargement of yellow dotted line square in (A). Scale bars, 5 μm. (**C**) Orthogonal view of isolated cardiomyocyte in (A) and (B). Original magnification, ×100; scale bars, 5 μm.

open-chest pigs, LV free wall biopsies from the beating heart were taken at baseline and sequentially after treatment. Three hundred minutes after inhalation, a marked HA signal was detected in the myocardium, providing evidence for effective delivery of CaP-HA to the heart (Fig. 4D). These data were supported by Western blot (Fig. 4E) and confocal microscopy (Fig. 4F) analyses of cardiac tissue. Together, these data confirm the efficiency of our CaP inhalation approach for intramyocardial delivery of compounds in a large animal.

DISCUSSION

Here, we provide the proof of concept for an innovative and unconventional nanotechnological inhalation approach for cardiac delivery of peptides for the treatment of pathological heart conditions. Inhalation per se has long been established for the treatment of pulmonary diseases (*26*, *27*), but its use for targeting of the heart and management of cardiac failing conditions has not previously been explored. We demonstrated that inhalation of our recently developed bioresorbable and negatively charged CaP nanocarriers (*15*) allows for effective targeting to and treatment of the heart, resulting in higher, faster, and more selective cardiac accumulation of CaPs compared to other delivery routes, such as gavage, intraperitoneal, or intravenous. The delivery of drugs through CaP-facilitated inhalation is thus likely to reduce the amount of required therapeutic compound, which, together with more cardiac-specific delivery, may minimize side effects compared to systemic delivery. Reduced first-pass metabolism may explain the more efficient delivery of CaPs to the heart by inhalation.

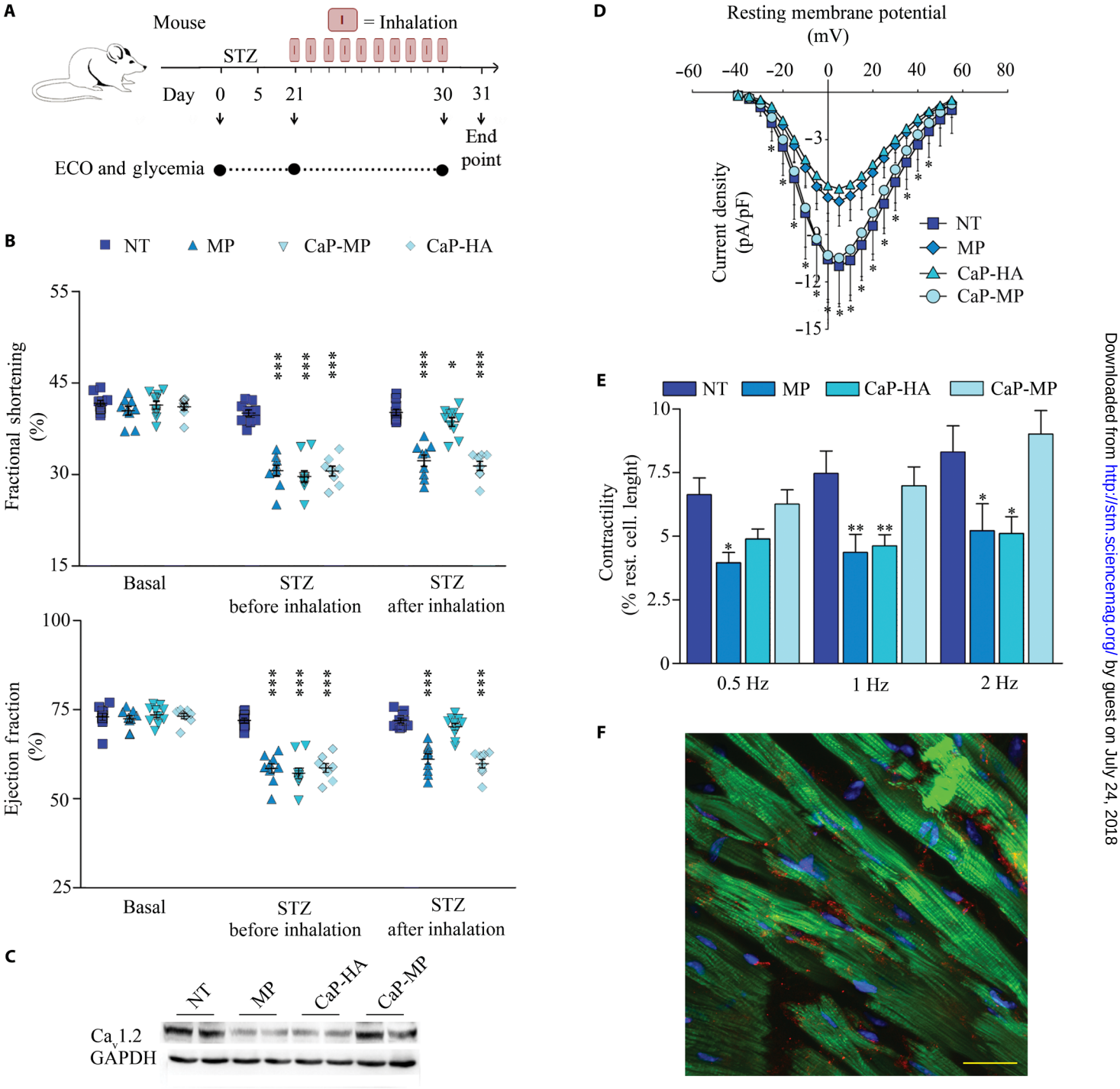

Fig. 3. Inhaled CaP-MPs restore cardiac function in a mouse model of diabetic cardiomyopathy. (**A**) Design of the study. ECO, echocardiography. (**B**) LV fractional shortening and ejection fraction (indices of cardiac contractile function) as determined by echocardiographic analysis on STZ-treated mice treated as indicated. Data are means ± SEM. ***$P < 0.001$ compared to NT mice (two-way ANOVA test) ($n = 10$). (**C**) Western blot analysis for the LTCC pore unit ($Ca_v\alpha1.2$) on adult cardiomyocytes isolated from treated mice. GAPDH, glyceraldehyde-3-phosphate dehydrogenase. (**D**) Average peak of LTCC current density as a function of voltage command measured in adult cardiomyocytes isolated from treated mice. All values are means ± SD for n cells. *$P < 0.02$ for NT compared to MP and CaP-HA mice ($n = 16$ to 21). (**E**) Contractility of adult cardiomyocytes isolated from treated mice. Data are means ± SEM. *$P < 0.05$ and **$P < 0.01$ compared to NT mice (two-way ANOVA test) ($n = 20$). (**F**) Z-stack confocal laser scanning microscopy images showing HA peptide in myocardial tissue from mouse treated by CaP-HA inhalation. Immunofluorescence staining for HA (red), LTCC (green), and cell nuclei [4′,6-diamidino-2-phenylindole (DAPI); blue]. Scale bar, 20 μm ($n = 3$).

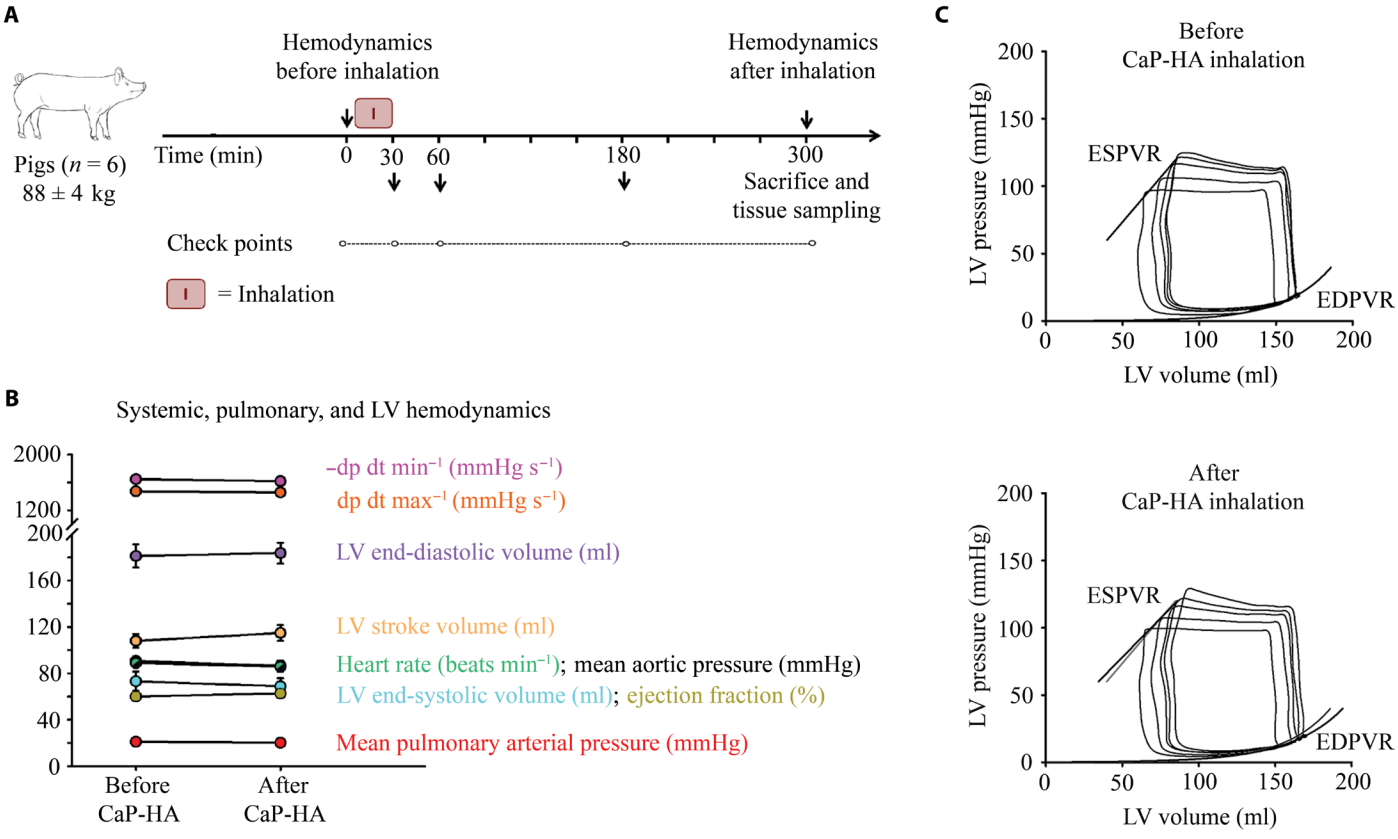

Fig. 4. CaP-HA inhalation in landrace pigs. (**A**) Design of the study. (**B**) Systemic, pulmonary, and LV hemodynamics ($n = 6$; data are means ± SEM). Steady-state data before and after CaP inhalation were compared by one-way ANOVA for repeated measurements. Pressure-volume relationships were compared by analysis of covariance. Post hoc testing was performed by Tukey's test. $P < 0.05$ was considered significant. (**C**) Original registrations from one representative animal of LV pressure-volume loops before (pre, top) and after (post, bottom) CaP-HA inhalation. All registrations were recorded at spontaneous heart rate. ESPVR, end-systolic pressure-volume relationship; EDPVR, end-diastolic pressure-volume relationship. (**D**) Kinetics of inhaled CaP-HA cardiac targeting as examined by dot blot analysis from biopsies obtained at the indicated times after inhalation. IB, immunoblotting. (**E**) Western blot analysis for HA on tissues of treated pigs. (**F**) Z-stack confocal laser scanning microscopy images showing HA peptide in myocardial tissue from pigs treated by CaP-HA inhalation. Immunofluorescence staining for HA (red), LTCC (green), and cell nuclei (DAPI; blue). Scale bar, 20 μm ($n = 6$).

Although the feasibility for a novel therapeutic application is envisaged, we acknowledge that some limitations are still present. For instance, pathological conditions affecting the lungs such as chronic obstructive pulmonary disease might affect CaP persistence and their translocation toward the pulmonary bloodstream, thereby limiting the efficiency of the targeted administration to the heart. In addition, the mechanistic events by which CaPs interact with and cross through the pulmonary barrier are still unknown and further efforts to understand these processes are necessary. CaPs might be subjected to physical modifications after in vivo administration. However, it is important to remark that no substantial size alterations occurred within the time required for CaPs to target the heart

after in vivo inhalation, which is within the first hours (fig. S1B). Last, despite our encouraging results, chronic administration and pharmacokinetic studies will be required to investigate the safety of this new delivery approach.

In conclusion, this study identifies an inhalation-based approach for targeting the heart and may open up new avenues of investigation and potential uses of nanomaterials for the treatment of CVD with therapeutic peptides. Inhalation therapy is easily administered and free from any physical or emotional burden associated with injection or other minimally invasive procedures, thus facilitating patient compliance, convenience, and home-based chronic treatment. A broader use of CaPs for carrying other drug/diagnostic compounds with different release kinetics (therapeutic polypharmacy) or even with different tissue targeting can be envisaged.

MATERIALS AND METHODS

Study design

The overall hypothesis is to target the diseased heart via inhaled nanoparticles carrying therapeutic peptides. Here, we designed a study to (i) synthesize a proper CaP-based MP carriers, (ii) test the effectiveness of CaP inhalation in small (mice), medium (rats), and large (pigs) animals, and (iii) treat a typical diabetes-induced cardiomyopathy via inhalation of CaP-MPs. In the setting for functional, histological, and molecular evaluations and cardiac activity monitoring, the number of animals per each individual group was minimized to 6 to 11 mice, 11 rats, and 9 pigs. For the therapeutic application, the sample size of diabetes-induced heart failure model was determined on the basis of previous experience (*24*) and taking into account the mortality rate. The study, which included 10 mice per individual group, was blinded and randomized. To ensure comparable degrees of cardiac dysfunction, noninvasive approaches such as echocardiography or ECG were assessed at each experimental time point. To ensure that neither the nanocarrier nor therapeutic peptide alone was responsible for the improved cardiac phenotype, we included mice that inhaled CaP-HA and MP, respectively. The large animal experiments were designed to achieve a proof of concept of the feasibility of our nanocarrier-mediated approach using a small number of animals (nine in total). The statistical analysis is therefore primarily descriptive in nature. The first series of animals was aimed at testing inhaled CaPs' ability to enrich the heart at a dose derived from previous experiments in rodents. After collecting evidence of heart enrichment via Western blotting, a separate set of animals was used to investigate the hemodynamic and electrophysiological effect of the carrier per se. Numbers were determined by the investigator according to previous experimental experience. All experimental procedures were approved by the Institutional Animal Care and Use Committee (permit no. 920/2015-PR, 746/2017-PR, 59/2012, and G0063/16) and conducted in accordance with the guidelines of the national councils where experiments were performed.

Nanoparticle preparation

CaPs were generated according to our previous work (*15*) through a biomineralization-inspired strategy consisting of mixing (1:1, v/v; 20 ml total) two aqueous solutions of (i) $CaCl_2$ (100 mM) + Na_3Cit (400 mM) and (ii) Na_2HPO_4 (120 mM) for 5 min at 37°C. pH was adjusted to 8.5 by adding 0.1 M NaOH. The mixed solution was kept in a water bath at 37°C for 5 min. For conjugation with the fluorophore, Sulfo-Cy7 amine (Lumiprobe GmbH) (125 μg/ml) was added, whereas for drug conjugation, HA or MP (500 μg/ml) (HA, YPYDVPDYA; MP, DQRPDREAPRS; GeneScript) was added. To remove unreacted reagents, the CaP suspension was dialyzed for 6 hours across a cellulose dialysis membrane with a cutoff of 3500 Da and immersed in 400 ml of Milli-Q water followed by multiple water exchanges. The suspension was recovered and stored at 4°C until further use. The final concentration of CaP suspensions was 600 μg/ml in all cases. The final concentrations of Cy7 and peptides within the CaP suspension were 75 and 150 μg/ml, respectively. Surface decoration of CaPs with Cy7 was also tested by adding an aqueous solution of Cy7 to the CaP suspension (final concentration of 15 μg/ml similar to the amount effectively encapsulated). The suspension was maintained overnight under shaking at 37°C. After that, the unadsorbed fluorophore was removed by extensive washings by centrifugation.

Nanoparticle characterization

The amount of CaPs after dialysis was evaluated by freeze-drying the sample suspensions (five aliquots of 1 ml) and weighing the solid content. The amount of HA and MP loaded on CaPs was detected using the DC Protein Assay (Bio-Rad) according to the manufacturer's instructions. The amount of Cy7 loaded on CaPs was measured using an ultraviolet-visible (UV-Vis) spectrophotometer (NanoDrop One, Thermo Scientific) ($\lambda = 750$ nm; $\varepsilon_{cy7} = 240{,}600\ M \cdot cm^{-1}$). The concentration of Cy7 was calculated as the difference between the concentration of the initial solution and that of the supernatant after sample centrifugation at 5000 rpm for 15 min. Size distribution and surface charge of unloaded and loaded CaPs were evaluated by dynamic light scattering (DLS) (Zetasizer Nano Series) and ζ-potential (Zetasizer Nano Analyzer) analysis, respectively. CaP particle size was measured by backscatter detection ($\lambda = 630$ nm; $\theta = 173°$) and reported as Z-average of hydrodynamic diameter of three measurements of 10 runs for 10 s at 25°C. The ζ-potential measurements through electrophoretic mobility were carried out using disposable folded capillary cells (DTS1061) at 25°C, suspending CaP in 10 mM Hepes buffer at pH 7.4. The ζ-potential was calculated from three separate measurements (100 runs each) in each case. TEM images were collected using an FEI Tecnai F20 ST microscope operating at 80 kV. An aliquot of 20 μl of nanoparticle suspension was placed on a carbon/formvar-coated copper grid for 5 min. The grid was then washed with ultrapure water and dried by manual blotting. The stability of CaP, CaP-MP, and CaP-HA in aqueous solution (600 μg/ml) starting immediately after dialysis was evaluated by measuring the Z-average and the surface charge of the suspensions as a function of time (up to 8 days) at 4°C by DLS and ζ-potential analysis. The stability of the unloaded CaP suspension 2 days after dialysis enriched with 10% (v/v) of FBS (Sigma-Aldrich) was also evaluated for up to 7 days at room temperature by DLS and ζ-potential analysis. The degradation of CaPs and CaP peptides at different pH values was evaluated by mixing 5 mg of freeze-dried nanoparticles with 10 ml of 0.1 M Hepes buffer solution (pH 7.4) or 10 ml of 0.1 M acetate buffer solution (pH 5.5). At scheduled times for up to 24 hours, 1 ml of the supernatant (that was well separated from the solid phase by 15 min of centrifugation at 5000 rpm) was removed for Ca^{2+} quantification and replaced with fresh buffer. Calcium content was determined by ICP-OES using a 5100 spectrometer (Agilent Technologies).

To evaluate peptide loading, the DC Protein Assay (Bio-Rad) was adopted according to the manufacturer's instructions. Quantification of both the pre- and post-dialysis preparations was performed from both pellet (CaP-MP) and supernatant (CaP-free MP) fractions obtained by centrifugation (14 min at 20,000*g*) of CaP-MPs. Before the

peptide quantification assay, both pellet and supernatant fractions were subjected to an acidic treatment (0.05 M HCl for 4 hours) to completely dissolve CaP-MPs and facilitate the total release and effective quantification of total MP.

The release of Cy7 from CaP-Cy7 was tested against an infinite sink in dialysis by transferring the particles into 3500-Da molecular weight cutoff cellulose membrane dialysis tubes and dialyzing against water for 24 hours with multiple water exchanges. At scheduled times, 10 μl of the supernatant (that was well separated from the solid phase by 15 min of centrifugation at 5000 rpm) was analyzed for fluorophore quantification using a UV-Vis spectrophotometer.

The release of Cy7 from CaP-Cy7 was also tested in aqueous solution (600 μg/ml) enriched with 10% (v/v) of FBS. At scheduled times, ranging from 1 min to 24 hours, 10 μl of the supernatant (that was well separated from the solid phase by 15 min of centrifugation at 5000 rpm) was analyzed for fluorophore quantification using a UV-Vis spectrophotometer.

Experimental animals

Mice

All procedures on mice were performed according to institutional guidelines in compliance with national (D.L. 04/03/2014, n.26) and international law and policies (directive 2010/63/EU). The protocol was approved by the Italian Ministry of Health. Special attention was paid to animal welfare and to minimize the number of animals used and their suffering. All experiments were performed on 10-week-old C57B6J male mice, CD1 male mice, and CD1-Foxn1 nude mice. All animals were obtained from the Charles River Laboratories. Therapeutic treatment of mice was performed as follows: Type 1 diabetes was induced in adult C57B6/J male mice by intraperitoneal injection of STZ (50 mg/kg per day) for five consecutive days as previously described (*24*). Seven days after the last STZ injection, whole blood was obtained from the mouse tail vein and glucose levels were measured using the Accu-Chek Aviva blood glucose monitoring system (Roche). Mice were fasted for 8 hours before blood collection. At 3 weeks after STZ treatment, mice were considered diabetic and used for the study only if glucose > 250 mg/dl and fractional shortening < 35% (29 of 36 STZ-treated mice were considered suitable for the study). STZ diabetic mice were randomly divided into three separate groups, and 50 μl of solution (CaP-MP, 0.5 mg/kg per day; CaP-HA, 0.5 mg/kg per day; MP, 0.5 mg/kg per day) was administered by inhalation via intratracheal nebulization for 10 consecutive days, as indicated.

Rats

The study population consisted of 11 male Wistar rats bred in the animal facility at the University of Parma, aged 12 to 14 weeks and weighing 300 to 350 g. Briefly, animals were anesthetized by intraperitoneal injection with a mixture of ketamine chloride (40 mg/kg) (Imalgene, Merial) and medetomidine hydrochloride (0.15 mg/kg) (Domitor, Pfizer Italia S.r.l.). All efforts were made to minimize suffering. This study was carried out in accordance with the recommendations in the *Guide for the Care and Use of Laboratory Animals* of the U.S. National Institutes of Health. The protocol was approved by the Veterinary Animal Care and Use Committee of the University of Parma and conforms to the National Ethical Guidelines of the Italian Ministry of Health (permit number: 59/2012).

Landrace pigs

The experimental protocol was approved by the local bioethics committee of Berlin, Germany (G 0063/16), and conforms to the *Guide for the Care and Use of Laboratory Animals* published by the U.S. National Institutes of Health (NIH publication no. 85-23, revised 1996). A total of nine healthy animals were anesthetized as previously described (*28*). Briefly, after administration of propofol (1 mg/kg), the animals were intubated and anesthesia was continued with 1 to 1.5% isoflurane, fentanyl (20 μg/kg per hour), and pancuronium (0.2 μg/kg per hour). The animals were ventilated (Cato, Dräger Medical) with an FiO_2 of 0.5, an inspiratory:espiratory ratio of 1:1.5, a positive end-expiratory pressure of 5 mmHg, and a tidal volume of 10 ml/kg. If necessary, the respiratory rate was adjusted to maintain an end-tidal carbon dioxide partial pressure between 35 and 40 mmHg. Sheath accesses of the left internal carotid artery and jugular vein were surgically prepared. Heart rate and arterial blood pressure were continuously monitored. A balanced crystalloid infusion (Sterofundin ISO, B. Braun Melsungen AG) was administered at a fixed rate of 10 ml/kg per hour throughout the protocol. A body temperature of 37.5° to 38.5°C was maintained by either surface cooling or a warming blanket.

Nanocarrier administration

Mice

CD1 mice were divided into four different groups of six mice, and 100 μl of CaP-Cy7 was administered by gavage, intraperitoneal, and intravenous injection (Cap-IP) as well as by intratracheal nebulization. For the intratracheal treatment, MicroSprayer Aerosolizer (model IA-1C) and FMJ-250 High Pressure Syringe (Penn-Century) were used. Mice were anesthetized with 3% isoflurane to allow nebulization. For each administration method, 11 mice administered with an aqueous Cy7 solution were used as controls. At the end of the experimentation, mice were sacrificed and tissues were collected.

Rats

Administration was performed via a 16-gauge catheter connected to a rodent ventilator (Rodent ventilator UB 7025, Ugo Basile) for artificial respiration. One dose (20 μl/100 g of body weight) of solution (CaP, 3 mg/kg, or saline) was administered via the catheter. After CaP administration, animals were woken up with a single intraperitoneal injection of atipamezole hydrochloride (0.15 mg/kg) (Antisedan, Pfizer) and left conscious for 4 hours before electrophysiological in vivo experiments were performed. Before exposing the heart, precordial ECGs (three unipolar and three bipolar leads) were recorded to screen for possible anoxic effects on cardiac electrical activity due to the tracheal instillation.

Landrace pigs

A left lateral thoracotomy was performed, and the left ventricle was exposed in a pericardial cradle. The protocol is described in Fig. 4A. After stabilization for 30 min, two transmural LV free wall biopsies were taken from the beating heart. Next, a 10-ml solution containing CaP-HA (10 mg/ml) (HA, 150 μg/ml) was nebulized over 30 min with the Aeroneb Professional Nebulizer System (Aeroneb Pro, Aerogen Ltd.), connected with an adult T-piece into the inspiratory limb of the breathing hoses. At 30, 60, 180, and 300 min after the beginning of inhalation, further biopsies were taken. All biopsies were rinsed carefully in saline, immediately frozen in liquid nitrogen, and stored at −80°C. Finally, the animals were sacrificed by a bolus injection of 100 mM potassium chloride, and samples were collected.

Echocardiography

A Vevo 2100 high-resolution in vivo imaging system (VisualSonics Fujifilm) with a MS550S probe "high frame" scan head was used for echocardiographic analysis. Mice were anesthetized with 1.0% isoflurane and imaged in M-mode as previously described (*24*).

Invasive hemodynamics in landrace pigs

A separate group of pigs ($n = 9$, 88 ± 4 kg; Fig. 4A) was acutely instrumented closed-chest under fluoroscopic guidance with a pulmonary artery flotation catheter [Continuous Cardiac Output (CCO) connected to Vigilance II, Edwards Lifesciences], an LV conductance catheter (5F, 12 electrodes, 7-mm spacing; MPVS Ultra, Millar Instruments), and a valvuloplasty catheter (24 ml; Osypka) in the descending aorta as previously described (*28*). A three-lead surface ECG was recorded throughout the whole experiment and used for offline analysis. Offline analysis included measurements of PQ intervals during spontaneous heart rates, QRS duration, and QT duration. After stabilization for 30 min, steady-state hemodynamics was acquired over three respiratory cycles. Pressure-volume relationships were generated by briefly inflating the intra-aortic balloon catheter three times. Next, a 10-ml solution containing CaP-HA (10 mg/ml) (HA, 150 μg/ml) was nebulized over 30 min with the Aeroneb Professional Nebulizer System as described above. Measurements were then repeated after 300 min. Pressure-volume data and time intervals were analyzed offline by CircLab software (custom-made by P. Steendijk). The conductance catheter measurements were calibrated by hypertonic saline solution (three boluses of 3 ml at 10%), and cardiac output was continuously derived from the pulmonary artery flotation catheter.

Statistical analysis

Assessment of normality of the data was calculated with the Kolmogorov-Smirnov test. Statistical comparisons were performed using one- or two-way ANOVA and Student's *t* test for unpaired samples in patch clamp experiments. Prism 6.0 software (GraphPad Software) was used to assess the normality of the data and for statistical calculation. A P value of <0.05 was considered significant unless otherwise indicated.

SUPPLEMENTARY MATERIALS

www.sciencetranslationalmedicine.org/cgi/content/full/10/424/eaan6205/DC1
Materials and Methods
Fig. S1. Size stability of CaPs and CaPs functionalized with MP and HA in protein-free and protein-enriched aqueous medium, and surface charge of CaP-Cy7 and CaPs with Cy7 adsorbed on their surface.
Fig. S2. In vivo and ex vivo characterization of CaPs.
Fig. S3. Echocardiographic analysis of CaP-treated mice.
Fig. S4. Stability, loading, degradation, and structural characterization of CaPs and CaPs functionalized with MP and HA.
Fig. S5. STED microscopy of isolated cardiomyocytes from mice treated with unloaded CaPs.
Fig. S6. MP-CaP treatment of diabetic mice.
Table S1. Echocardiographic analysis of 10-week-old male wild-type mice treated with CaP.
Table S2. Excitability and refractoriness parameters obtained by epicardial multiple lead recording in untreated rats or rats treated with CaP.
Table S3. CaP-MP loading.
Table S4. Echocardiographic analysis of 10-week-old male wild-type and STZ mice treated with MP, CaP-HA, and CaP-MP.
Table S5. Characterization of LTCC current during rectangular double-pulse protocols and membrane capacities measured in adult cardiomyocytes isolated from treated mice.
Table S6. Thiobarbituric acid–reactive substance detection in mice treated with MP, CaP-HA, and CaP-MP.
Movie S1. 3D FMT imaging of the cardiopulmonary area from Cy7-treated mice.
Movie S2. 3D FMT imaging of the cardiopulmonary area from CaP-Cy7–treated mice.
Movie S3. STED microscopy of isolated cardiomyocytes from mice treated with MP-rhodamine–loaded CaPs.

REFERENCES AND NOTES

1. M. Giardiello, N. J. Liptrott, T. O. McDonald, D. Moss, M. Siccardi, P. Martin, D. Smith, R. Gurjar, S. P. Rannard, A. Owen, Accelerated oral nanomedicine discovery from miniaturized screening to clinical production exemplified by paediatric HIV nanotherapies. *Nat. Commun.* **7**, 13184 (2016).
2. B. Y. S. Kim, J. T. Rutka, W. C. W. Chan, Nanomedicine. *N. Engl. J. Med.* **363**, 2434–2443 (2010).
3. M. E. Davis, J. E. Zuckerman, C. H. J. Choi, D. Seligson, A. Tolcher, C. A. Alabi, Y. Yen, J. D. Heidel, A. Ribas, Evidence of RNAi in humans from systemically administered siRNA via targeted nanoparticles. *Nature* **464**, 1067–1070 (2010).
4. V. Weissig, T. K. Pettinger, N. Murdock, Nanopharmaceuticals (part 1): Products on the market. *Int. J. Nanomed.* **9**, 4357–4373 (2014).
5. R. Kuai, L. J. Ochyl, K. S. Bahjat, A. Schwendeman, J. J. Moon, Designer vaccine nanodiscs for personalized cancer immunotherapy. *Nat. Mater.* **16**, 489–496 (2017).
6. Y. Zhao, F. Fay, S. Hak, J. Manuel Perez-Aguilar, B. L. Sanchez-Gaytan, B. Goode, R. Duivenvoorden, C. de Lange Davies, A. Bjørkøy, H. Weinstein, Z. A. Fayad, C. Pérez-Medina, W. J. M. Mulder, Augmenting drug–carrier compatibility improves tumour nanotherapy efficacy. *Nat. Commun.* **7**, 11221 (2016).
7. E. Blanco, H. Shen, M. Ferrari, Principles of nanoparticle design for overcoming biological barriers to drug delivery. *Nat. Biotechnol.* **33**, 941–951 (2015).
8. Y. T. Ho, B. Poinard, J. C. Y. Kah, Nanoparticle drug delivery systems and their use in cardiac tissue therapy. *Nanomedicine* **11**, 693–714 (2016).
9. C. W. Evans, K. S. Iyer, L. C. Hool, The potential for nanotechnology to improve delivery of therapy to the acute ischemic heart. *Nanomedicine* **11**, 817–832 (2016).
10. S. S. Behera, K. Pramanik, M. K. Nayak, Recent advancement in the treatment of cardiovascular diseases: Conventional therapy to nanotechnology. *Curr. Pharm. Des.* **21**, 4479–4497 (2015).
11. S. Mendis, S. Davis, B. Norrving, Organizational update: The world health organization global status report on noncommunicable diseases 2014; one more landmark step in the combat against stroke and vascular disease. *Stroke* **46**, e121–e122 (2015).
12. S. Suarez, A. Almutairi, K. L. Christman, Micro- and nanoparticles for treating cardiovascular disease. *Biomater. Sci.* **3**, 564–580 (2015).
13. K. Fosgerau, T. Hoffmann, Peptide therapeutics: Current status and future directions. *Drug Discov. Today* **20**, 122–128 (2015).
14. T. Uhlig, T. Kyprianou, F. G. Martinelli, C. A. Oppici, D. Heiligers, D. Hills, X. R. Calvo, P. Verhaert, The emergence of peptides in the pharmaceutical business: From exploration to exploitation. *EuPA Open Proteom.* **4**, 58–69 (2014).
15. V. Di Mauro, M. Iafisco, N. Salvarani, M. Vacchiano, P. Carullo, G. B. Ramírez-Rodríguez, T. Patrício, A. Tampieri, M. Miragoli, D. Catalucci, Bioinspired negatively charged calcium phosphate nanocarriers for cardiac delivery of microRNAs. *Nanomedicine* **11**, 891–906 (2016).
16. M. Savi, S. Rossi, L. Bocchi, L. Gennaccaro, F. Cacciani, A. Perotti, D. Amidani, R. Alinovi, M. Goldoni, I. Aliatis, P. P. Lottici, D. Bersani, M. Campanini, S. Pinelli, M. Petyx, C. Frati, A. Gervasi, K. Urbanek, F. Quaini, A. Buschini, D. Stilli, C. Rivetti, E. Macchi, A. Mutti, M. Miragoli, M. Zaniboni, Titanium dioxide nanoparticles promote arrhythmias via a direct interaction with rat cardiac tissue. *Part. Fibre Toxicol.* **11**, 63 (2014).
17. N. L. Mills, K. Donaldson, P. W. Hadoke, N. A. Boon, W. MacNee, F. R. Cassee, T. Sandström, A. Blomberg, D. E. Newby, Adverse cardiovascular effects of air pollution. *Nat. Clin. Pract. Cardiovasc. Med.* **6**, 36–44 (2009).
18. M. Miragoli, P. Novak, P. Ruenraroengsak, A. I. Shevchuk, Y. E. Korchev, M. J. Lab, T. D. Tetley, J. Gorelik, Functional interaction between charged nanoparticles and cardiac tissue: A new paradigm for cardiac arrhythmia? *Nanomedicine* **8**, 725–737 (2013).
19. S. Bakand, A. Hayes, F. Dechsakulthorn, Nanoparticles: A review of particle toxicology following inhalation exposure. *Inhal. Toxicol.* **24**, 125–135 (2012).
20. W. H. De Jong, P. J. Borm, Drug delivery and nanoparticles: Applications and hazards. *Int. J. Nanomed.* **3**, 133–149 (2008).
21. J. R. Roberts, W. McKinney, H. Kan, K. Krajnak, D. G. Frazer, T. A. Thomas, S. Waugh, A. Kenyon, R. I. MacCuspie, V. A. Hackley, V. Castranova, Pulmonary and cardiovascular responses of rats to inhalation of silver nanoparticles. *J. Toxicol. Environ. Health A* **76**, 651–668 (2013).
22. L. Petrick, M. Rosenblat, N. Paland, M. Aviram, Silicon dioxide nanoparticles increase macrophage atherogenicity: Stimulation of cellular cytotoxicity, oxidative stress, and triglycerides accumulation. *Environ. Toxicol.* **31**, 713–723 (2016).
23. K. Lin, C. Wu, J. Chang, Advances in synthesis of calcium phosphate crystals with controlled size and shape. *Acta Biomater.* **10**, 4071–4102 (2014).
24. F. Rusconi, P. Ceriotti, M. Miragoli, P. Carullo, N. Salvarani, M. Rocchetti, E. Di Pasquale, S. Rossi, M. Tessari, S. Caprari, M. Cazade, P. Kunderfranco, J. Chemin, M.-L. Bang, F. Polticelli, A. Zaza, G. Faggian, G. Condorelli, D. Catalucci, Peptidomimetic targeting of $Ca_v\beta2$ overcomes dysregulation of the L-type calcium channel density and recovers cardiac function. *Circulation* **134**, 534–546 (2016).
25. L. P. Kozlowski, IPC—Isoelectric point calculator. *Biol. Direct* **11**, 55 (2016).
26. J. S. Patton, C. S. Fishburn, J. G. Weers, The lungs as a portal of entry for systemic drug delivery. *Proc. Am. Thorac. Soc.* **1**, 338–344 (2004).
27. M. Irngartinger, V. Camuglia, M. Damm, J. Goede, H. W. Frijlink, Pulmonary delivery of therapeutic peptides via dry powder inhalation: Effects of micronisation and manufacturing. *Eur. J. Pharm. Biopharm.* **58**, 7–14 (2004).

28. A. Alogna, M. Manninger, M. Schwarzl, B. Zirngast, P. Steendijk, J. Verderber, D. Zweiker, H. Maechler, B. M. Pieske, H. Post, Inotropic effects of experimental hyperthermia and hypothermia on left ventricular function in pigs—Comparison with dobutamine. *Crit. Care Med.* **44**, e158–e167 (2016).

Acknowledgments: We acknowledge M.-L. Bang for critically reading the manuscript. **Funding:** This study was supported by the Italian Ministry of Education, Universities, and Research flagship Nanomax, 2013-2017, to D.C., M.M., and A.T.; H2020-NMBP-2016 720834 CUPIDO (www.cupidoproject.eu) to D.C., M.M., M.I., and H.P.; and Italian Ministry of Health GR-2011-02352546 to D.C. **Author contributions:** P. Ceriotti, M.V., N.S., A.A., P. Carullo, M.E., G.B.R.-R., T.P., L.D.E., S.P., S.R., H.P., and M.M. carried out experiments. In particular, P. Ceriotti carried out several of the experiments and analyses; N.S., S.R., and M.M. were responsible for electrophysiology studies and analyses; M.V. performed all mouse setups and treatments, physiological analyses, and graphic representations; P. Carullo performed echocardiographic analyses and cardiomyocyte isolation; M.V. and M.E. performed in vivo imaging; M.E. performed STED; F. Rossi and F. Ravanetti performed TEM on cardiac cells and tissue; H.P. and A.A. performed the large animal experiments; P. Ceriotti, G.B.R.-R., T.P., and L.D.E. prepared and characterized nanoparticle formulations; S.P. and R.A. performed T-bars analysis; M.I. designed and supervised the synthesis and functionalization of nanoparticles; M.M. and D.C. designed the study and supervised most of the experiments; M.M., M.I., G.C., and D.C. wrote the manuscript; A.T., H.P., M.M., M.I., and D.C. acquired funding for the study. **Competing interests:** D.C. and G.C. are authors on patent application no. MI2014A000097 and PCT/EP2015/051376 (WO2015/110589) "Mimetic peptides and their use in medicine" submitted by the Italian National Research Council, which covers MPs that, through a novel mechanism, directly target the LTCC and are suitable for use in the treatment of conditions where LTCC density and function are altered. D.C., M.M., M.I., and A.T. are authors on patent application no. MI2014A002207 and PCT/EP2015/080991 (WO2016/102576) "Products for the delivery of therapeutic/diagnostic compounds to the heart" submitted by the Italian National Research Council (75%) and the Italian Istituto nazionale Assicurazione Infortuni sul Lavoro (25%), which covers a process for the preparation of a product comprising one or more nanoparticles of CaP that are suitable for use as a vehicle for one or more diagnostic/therapeutic compounds for the treatment of CVDs through inhalation administration. The other authors declare that they have no competing interests. **Data and materials availability:** All data reported in the paper are included in the manuscript or available in the Supplementary Materials. Requests for materials (CaPs; MP and scramble peptides) should be addressed to D.C. (daniele.catalucci@cnr.it) and will be handled according to a material transfer agreement through the Italian National Research Council.

Submitted 11 May 2017
Resubmitted 17 August 2017
Accepted 29 November 2017
Published 17 January 2018
10.1126/scitranslmed.aan6205

Citation: M. Miragoli, P. Ceriotti, M. Iafisco, M. Vacchiano, N. Salvarani, A. Alogna, P. Carullo, G. B. Ramirez-Rodríguez, T. Patrício, L. D. Esposti, F. Rossi, F. Ravanetti, S. Pinelli, R. Alinovi, M. Erreni, S. Rossi, G. Condorelli, H. Post, A. Tampieri, D. Catalucci, Inhalation of peptide-loaded nanoparticles improves heart failure. *Sci. Transl. Med.* **10**, eaan6205 (2018).

Science Translational Medicine

Inhalation of peptide-loaded nanoparticles improves heart failure

Michele Miragoli, Paola Ceriotti, Michele Iafisco, Marco Vacchiano, Nicolò Salvarani, Alessio Alogna, Pierluigi Carullo, Gloria Belén Ramirez-Rodríguez, Tatiana Patrício, Lorenzo Degli Esposti, Francesca Rossi, Francesca Ravanetti, Silvana Pinelli, Rossella Alinovi, Marco Erreni, Stefano Rossi, Gianluigi Condorelli, Heiner Post, Anna Tampieri and Daniele Catalucci

Sci Transl Med **10**, eaan6205.
DOI: 10.1126/scitranslmed.aan6205

A puff of particles for the heart

Nanoparticles can be useful for imaging and drug delivery but generally require intravenous injection to reach their targets. Miragoli *et al*. delivered nanoparticles carrying peptides to the heart by inhalation rather than injection. The inhaled particles reached the heart faster than injected particles and were taken up by cardiomyocytes to improve cardiac function in a mouse model of diabetic cardiomyopathy. In healthy pigs, inhaled particles were also found in heart tissue, suggesting that this minimally invasive method of targeted cardiac delivery could potentially translate to humans.